

The optical modules of the phase-2 of the NEMO project

This content has been downloaded from IOPscience. Please scroll down to see the full text.

2013 JINST 8 P07001

(<http://iopscience.iop.org/1748-0221/8/07/P07001>)

View [the table of contents for this issue](#), or go to the [journal homepage](#) for more

Download details:

IP Address: 192.84.134.230

This content was downloaded on 15/07/2014 at 14:15

Please note that [terms and conditions apply](#).

The optical modules of the phase-2 of the NEMO project

S. Aiello,^a E. Leonora,^{a,1} F. Ameli,^b M. Anghinolfi,^c A. Anzalone,^d G. Barbarino,^e E. Barbarito,^f F. Barbato,^e A. Bersani,^c N. Beverini,^t S. Biagi,^o M. Bonori,^u B. Bouhadef,^s C. Bozza,ⁱ G. Cacopardo,^d A. Capone,^u F. Caruso,^d A. Ceres,^m T. Chiarusi,ⁿ M. Circella,^m R. Cocimano,^d R. Coniglione,^d M. Cordelli,^l M. Costa,^d A. D'Amico,^d R. De Asmundis,^r G. De Bonis,^b G. De Rosa,^e R. De Vita,^c C. Distefano,^d P. Fermani,^u V. Flaminio,^t L.A. Fusco,ⁿ F. Garufi,^e V. Giordano,^a G. Giovanetti,^{d,1} G. Grella,ⁱ A. Grimaldi,^a R. Habel,^l M. Imbesi,^d V. Kulikovskiy,^c D. Lattuada,^d G. Leotta,^h A. Lonardo,^b F. Longhitano,^a D. Lo Presti,^q E. Maccioni,^t A. Margiotta,^o A. Marinelli,^t A. Martini,^l R. Masullo,^u F. Maugeri,^d P. Migliozi,^r E. Migneco,^d S. Minutoli,^c A. Miraglia,^d C. Mollo,^r M. Mongelli,^m M. Morganti,^e P. Musico,^c M. Musumeci,^d C.A. Nicolau,^b A. Orlando,^d R. Papaleo,^d V. Pappalardo,^d C. Pellegrino,^d C. Perrina,^u P. Piattelli,^d C. Pugliatti,^q S. Pulvirenti,^d F. Raffaelli,^e G. Raia,^d N. Randazzo,^a G. Riccobene,^d A. Rovelli,^d A. Russo,^e G. V.Russo,^q P. Sapienza,^d D. Sciliberto,^a M. Sedita,^d I. Sgura,^m E. Shirokov,^c F. Simeone,^u V. Sipala,^p C. Sollima,^s M. Spina,^d M. Spurio,^o F. Stefani,^t M. Taiuti,^c G. Terreni,^s L. Trasatti,^g A. Trovato,^d P. Vicini,^b S. Viola^d and D. Vivolo^e

^aINFN Sezione di Catania,

Via S.Sofia 64, 95123 Catania, Italy

^bINFN Sezione di Pisa and Dipartimento di Fisica Università di Pisa, Polo Fibonacci,

Largo B.Pontecorvo 3, 56127 Pisa, Italy

^cINFN Sezione di Genova,

Via Dodecaneso 33, 16146 Genova, Italy

^dINFN, Laboratori Nazionali del Sud,

Via S.Sofia 62, 95123 Catania, Italy

^eINFN Sezione di Napoli,

Via Cintia, 80126 Napoli, Italy

^fINFN Sezione di Bari and Dipartimento Interateneo di Fisica Università di Bari,

Via E.Orabona 4, 70126 Bari, Italy

¹Corresponding author.

²Now at INGV, Roma, Italy

^gAccademia Navale di Livorno,
viale Italia 72, 57100 Livorno, Italy

^hDipartimento di Fisica e Astronomia Università di Catania,
Via S.Sofia 64, 95123 Catania, Italy

ⁱDipartimento di Fisica Università di Salerno and INFN Gruppo Collegato di Salerno,
Via Ponte Don Melillo, 84084 Fisciano, Italy

^lINFN Laboratori Nazionali di Frascati,
Via Enrico Fermi 40, 00044 Frascati(RM), Italy

^mINFN Sezione di Bari,
Via E.Orabona 4, 70126 Bari, Italy

ⁿINFN Sezione di Bologna,
V.le Bertini Pichat 6/2, 40127 Bologna, Italy

^oINFN Sezione di Bologna and Dipartimento di Fisica Università di Bologna,
V.le Bertini Pichat 6/2, 40127 Bologna, Italy

^pINFN Sezione di Cagliari and Dipartimento di Chimica e Farmacia - Università degli Studi di Sassari,
Via Vienna 2, 07100 Sassari, Italy

^qINFN Sezione di Catania and Dipartimento di Fisica e Astronomia Università di Catania,
Via S.Sofia 64, 95123 Catania, Italy

^rINFN Sezione di Genova and Dipartimento di Fisica Università di Genova,
Via Dodecaneso 33, 16146 Genova, Italy

^sINFN Sezione di Napoli and Dipartimento di Scienze Fisiche Università di Napoli,
Via Cintia, 80126 Napoli, Italy

^tINFN Sezione di Pisa,
Polo Fibonacci, Largo B.Pontecorvo 3, 56127 Pisa, Italy

^uINFN Sezione di Roma1,
P.le A.Moro 2, 00185 Roma, Italy

^vINFN Sezione di Roma1 and Dipartimento di Fisica Università di Roma "La Sapienza",
P.le A.Moro 2, 00185 Roma, Italy

E-mail: Emanuele.Leonora@ct.infn.it

ABSTRACT: A 13-inch Optical Module (OM) containing a large-area (10-inch) photomultiplier was designed as part of Phase-2 of the NEMO project. An intense R&D activity on the photomultipliers, the voltage supply boards, the optical coupling as well as the study of the influences of the Earth's magnetic field has driven the choice of each single component of the OM. Following a well-established production procedure, 32 OMs were assembled and their functionality tested. The design, the testing and the production phases are thoroughly described in this paper.

KEYWORDS: Cherenkov detectors; Optical detector readout concepts; Instrument optimisation; Large detector systems for particle and astroparticle physics

Contents

1	Introduction	1
2	The NEMO phase-2 optical module	2
2.1	The transparent high-pressure vessel	3
2.2	The photomultiplier	4
2.2.1	Ageing effect characterization	5
2.3	The high voltage supply board	6
2.4	The magnetic shielding	7
2.5	The optical coupling	11
2.6	The front end module	13
2.7	The time calibration system	13
3	Non-standard optical modules	14
3.1	PORFIDO	14
3.2	LED beacon	15
3.3	Piezo-electric acoustic transducers	16
4	The optical module production procedures	16
4.1	The optical module assembly	16
4.2	The optical module testing	17
4.3	The optical module sealing	18
4.4	Test under pressure	18
5	Conclusions	18

1 Introduction

The main goal of high-energy neutrino telescopes is the study of the Universe by observing extremely high-energy neutrinos ($10^{11} - 10^{16}$ eV) [1, 2]. The most suitable technique to perform such measurement is to instrument large volumes of water (or ice) in order to detect the Cherenkov radiation emitted by the secondary muons and hadrons produced in the neutrino interactions with the matter surrounding the detector [3]. This light can be detected by using a three-dimensional array of Optical Modules (OMs) [4]. The measurement of the arrival time of the light at the different OMs, whose positions are known, allows reconstructing the muon direction. The amount of light collected can be used to estimate the particle energy.

The NEMO (NEutrino Mediterranean Observatory) [5] has been active in the R&D activities needed for the ambitious goal of building a very large neutrino telescope, with a size of several km^3 , in the Mediterranean Sea. In the period 1998-2004 the activities were mainly focused at the

identification and characterization of a deep-sea site suitable for detector installation as well as at the development of the technology for such a large detector. A site with optimal features in terms of depth (3500 m) and water optical properties was identified at about 80 km offshore Capo Passero, in Sicily [6].

The so-called Phase-1 of the NEMO project, carried out in the period 2004-2007, consisted in a test of the technological solutions proposed for the building block of the detector, the tower. The prototype developed for Phase-1 was a “mini-tower” of 4 floors, each one consisting in a 15 m long structure hosting two OMs each end, looking downwards and horizontally. The OM consisted of a 10-inch PMT housed inside a 17-inch pressure resistant glass sphere. The vertical space between floors was 40 m. This apparatus was deployed at 2000 m depth at the Underwater Test Site of the Laboratori Nazionali del Sud (LNS) in Catania, connected to the shore by means of a 28 km electro-optical cable and operated for about 6 months [7].

Subsequently, the NEMO Collaboration launched a Phase-2 of the project. One the aim was the development of a new infrastructure in the Capo Passero deep-sea site. Such infrastructure, that is now fully operating, consists of a shore station, located inside the harbour area of Portopalo di Capo Passero, a 100 km electro-optical cable, which links the 3500 m deep-sea site to the shore station, and an underwater junction box needed to connect the detector.

As part of this project, a fully equipped 8-storey tower, to be installed at the deep-sea site, was designed and constructed. As in the Phase-1 tower, each storey hosts 2 optical modules at each end, oriented downwards and horizontally. In order to optimize the design of the mechanical structure the length of the storey is reduced to 8 m and the OM glass sphere diameter to 13-inch, still using 10-inch PMT. The design and the production of the OMs, the key element of this detector, are described in this paper.

2 The NEMO phase-2 optical module

The scientific goals of the NEMO project define the global requirements for the OMs. The mean intensity of the Cherenkov light signal, which arrives at each OM, could be as low as few photons. To optimize of the photon sensitive area inside the OM is therefore mandatory a large diameter PMT has been adopted (10 inch). The OM must satisfy the following requirements:

- the PMT must be enclosed in a transparent pressure-resistant container;
- the optical coupling between the water and the photocathode has to be optimized;
- the influence of the Earth’s magnetic field must be minimized;
- electronic boards like PMT power supply, front end electronics and calibration devices must be installed inside the OM vessel;
- all the components must be highly reliable. Indeed, the neutrino telescope lifetime must be larger than 10 years without major maintenance.

As shown in figure 1, the optical module designed for NEMO Phase-2 has a large-area, 10-inch-diameter PMT glued inside a 13-inch pressure resistant glass sphere by means of an optical gel. A

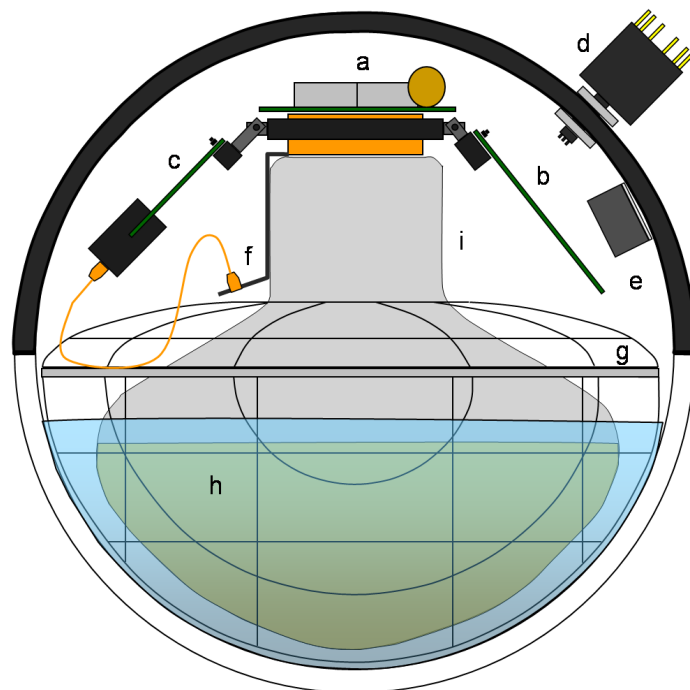


Figure 1. Schematic view of the main components of an optical module: (a) voltage divider circuit; (b) Front-end module (FEM); (c) fast optical pulser of the Tim-Cal; (d) feed trough connector; (e) pressure-gauge; (f) optical fibre; (g) mu-metal cage; (h) optical gel; (i) PMT.

mu-metal wire cage is used as a shield against the Earth’s magnetic field. Inside the OM also the voltage supply circuit soldered to the PMT, the Front End Module (FEM) and an optical system for Timing Calibration (Tim-Cal) are housed. An extensive R&D study has been carried out over the past few years in order to select each element of the optical module and to optimize the production procedure. This work is summarized in the following sections.

2.1 The transparent high-pressure vessel

The requirements for the high-pressure vessel of the optical module are:

- capability to withstand hydrostatic pressure, up to 400 atm;
- transparency to photons in the 350-600 nm wavelength range and a refractive index that ensures a good optical matching between the sea-water and the PMT.

A standard 13-inch spherical deep-sea instrumentation vessel in borosilicate glass, produced by Nautilus¹ was selected. This sphere is smaller than the 17-inch vessel adopted in Phase-1 of the NEMO project inline of the choice made by the ANTARES project [8].

Indeed, many tests proved that a 10-inch PMT could be safely contained in a smaller vessel. This solution simplifies many technical and mechanical aspects of the tower construction.

Each glass sphere is composed by two hemi-spherical halves: one supports the PMT and the mu-metal cage, glued to the glass inner surface using an optical gel. The inner surface of the second

¹Nautilus Marine Service GmbH, Heferwende 3, D-28357 Bremen, Germany, web-site: www.nautilus-gmbh.de

Table 1. Main properties of the glass vessel (Nautilus).

Refractive index	1.48
Specific gravity at 25 C [g/cm^3]	2.23
Outer diameter [mm / inch]	330/13
Glass thickness [mm]	12
Weight in air [kg]	8.6
Depth rating [m]	7000

halve is painted in black to stop the photons impinging from the back. A pressure gauge is glued onto the inner surface of the back hemisphere to monitor the pressure inside the OM. A 12-pin SEA CON[®]² feed through, also mounted on the back hemisphere, provides electrical connections (see figure 1). The main characteristics of the glass vessel (Nautilus VITROVEX[®] NMS-IS-7000) are summarised in table 1.

2.2 The photomultiplier

The PMTs are the active elements of a Cherenkov detector. They allow to measure photon radiation of the light impinging on the photocathode and the time of occurrence of this event.

Uncertainties in the measurement of the hit time affect the track reconstruction while uncertainties on the charge reconstruction affect mainly the evaluation of the energy of the charged particle that originated the Cherenkov radiation.

Any PMT pulse that is not related to the Cherenkov radiation affect the efficiency in track reconstruction. Spurious pulses, originated inside the PMT and correlated with a true signal, can affect seriously the track reconstruction. These noise pulses can be classified into four groups according to their causes and arrival times. For details see [9]. Pre-pulses appear 10-80 ns before the main pulse, in place of it. Late pulses appear 10-80 ns after the main pulse, in place of it. Type 1 after pulses appear in the 10-80 ns interval time after the main pulses. Type 2 after pulses arrive in the 80ns-16 μ s interval time after the main pulses. The percentage of spurious pulses indicates the ratio between the number of spurious pulses with respect to the numbers of main pulse. As already mentioned, for the NEMO Phase-2 detector was decided to use a 10-inch PMT satisfying the following characteristics:

- single photon detection capability;
- gain $\approx 5 \cdot 10^7$, with a nominal voltage lower than 2000 V;
- timing resolution better than 3 ns (as FWHM);
- Peak to Valley (P/V) ratio greater than 2;
- charge resolution better than 50% (as sigma);
- dark count rate smaller than 5 kHz;

²SEA CON[®] 1700 Gillespie Way, El Canjon, CA 92020, USA web-site: <http://seaconword.com>

Table 2. Mean values of different quantities obtained from the measurements of 72 R7081 PMTs. The NEMO pre-required values are shown in the last column.

	mean value	values required
Voltage at Gain $5 \cdot 10^7$ [V]	1655	< 2000
Dark Count rate [Hz] (1/3 s.p.e)	1388	< 5000
P/V ratio	3.5	> 2
Charge resolution σ [%]	31.6	< 50
TTS FWHM [ns]	2.8	< 3
Pre-Pulse [%]	0.02	< 1
Late-Pulse [%]	5.5	< 5
Type 1 after pulse [%]	1.1	< 1
Type 2 after pulse [%]	4.4	< 5

- pre-pulse percentage lower than 1%;
- late-pulse percentage lower than 5%;
- type 1 and type 2 after-pulses percentage smaller than 1% and 5% respectively.

Given these requirements, different types of photomultipliers from various manufacturers were tested. Finally, a Hamamatsu³ PMT type R7081 sel. was selected. It has 10-stages and a 10-inch bialkali photocathode with a typical surface around 500 cm^2 and a quantum efficiency of about 25% at 400 nm wavelength. Moreover, the PMTs for the NEMO project were selected among standard R7081 tubes by requiring a low fraction of spurious pulses and a low operating voltage to achieve gains of the order of $5 \cdot 10^7$. Measurements and acceptance tests were carried out on a batch of 72 PMTs. The whole photocathode surface was illuminated with a pulsed laser set in single photoelectron (s.p.e) condition. All the PMTs were powered with the voltage supply circuit described in section 2.3. Details on the measurements may be found in [9]. Results show that the measured PMT characteristics satisfy the requirements in term of P/V ratio, charge resolution, Transit Time Spread (TTS), dark count rate and frequency of spurious pulses. Table 2 summarizes the requirements and the mean values obtained from the measurements on the 72 PMTs.

2.2.1 Ageing effect characterization

During underwater operations, the OMs are exposed to a continuous optical background due to ^{40}K decays plus a contribution due to the diffuse bioluminescence. Measurements, taken during NEMO Phase-1 with 10-inch PMT at 3500 deep Capo Passero site, showed typical values of optical background of the order of 30 kHz, with values exceeding 200 kHz for less than 0.5% fraction of the operating time [10]. An accurate study of the aging effects was performed for almost three years on a 10-inch R7081 sel. PMT. The aging measurements consisted of cycles of two different phases: an accelerated ageing phase and a full characterization of the PMT in s.p.e. condition. During the

³ Hamamatsu Photonics, 812 joko-cho, Hamamatsu city,431-31 Japan, web-site: www.hamamatsu.com

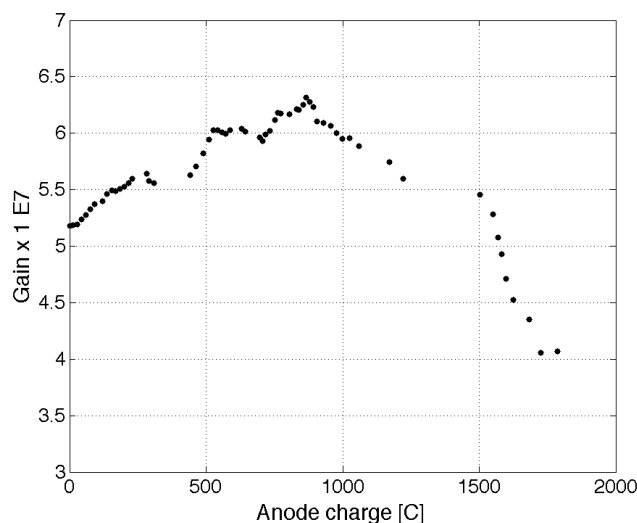


Figure 2. Ageing effect of the gain as a function of the total charge accumulated.

first phase the photocathode was illuminated with a 400 nm LED producing pulsed signals with an average value of about 3 photoelectrons at a frequency of 1 MHz. Thus, the full period of almost 3-years of measurement turns out to be equivalent to about 45 years of operative life of a PMT under an exposure of 1 s.p.e. at 200 kHz. Typically once a week the PMT ageing phase was interrupted and a characterization phase was carried out. During the characterization phase a pulsed laser source of 400 nm wavelength, set in s.p.e. condition was used to illuminate the whole photocathode surface in order to measure the gain, the time and the charge characteristics as well as the spurious pulses. The measurements showed that all the PMTs parameters, with the exception of the gain, did not change substantially during long operating periods. The gain as a function of the anode charge accumulated during the ageing test, up to about 1800 C, is shown in figure 2. After an initial gain increase of about 10%, with respect to the initial value of $5 \cdot 10^7$, a sharp decrease of the gain of about 30% is observed for larger values of the accumulated anode charge. This result is in agreement with a model that describes the ageing effects as due to a progressive sputtering of the excess caesium layer on the final dynodes by means of the secondary electron flow [11].

2.3 The high voltage supply board

The high voltage system provides all the intermediate voltages necessary for the correct operation of the PMT. A version of PHQ7081-i-2m integrated active board produced by ISEG⁴ and modified following the NEMO requirement was chosen. Damping resistors, whose values were chosen by the NEMO to minimize the ringing effect on the anode signal, were added by ISEG to the last output stages of the board. The high voltage is generated on the board by using a Cockroft-Walton scheme that requires only a low voltage supply. This has the advantage of reducing power consumption and making the design more compact. The main features of the system are:

- a low voltage supply of +5 V DC;

⁴ISEG Bautzer Landstr. 23, 01454 Radeberg / OT Rossendorf, Germany

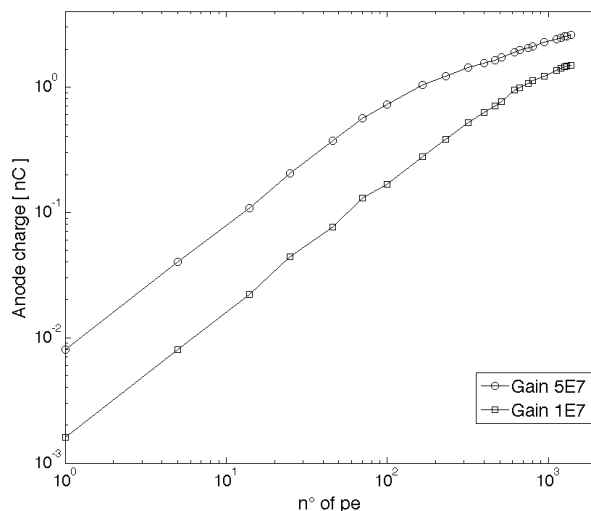


Figure 3. Anode charge as a function of the light intensity for two different gains: $5 \cdot 10^7$ (open circles) and $1 \cdot 10^7$ (open squares).

- a controllable focusing voltage between the photo-cathode and first-dynode (set at 700 V);
- an anode max current over 100 mA;
- a power consumption of 150 mW at 2000 V.

Tests performed by using two different gains ($1 \cdot 10^7$ and $5 \cdot 10^7$) showed that, for the R7081 PMT powered by the ISEG board and illuminated with laser-light pulses with a width of 60 ps (FWHM), the signal saturation starts at around 1 nC, see figure 3.

2.4 The magnetic shielding

The performance of a PMT is strongly affected by magnetic fields. This is particularly true for large area PMTs where photoelectrons travel long trajectories [12]. Therefore, the performance of the selected PMT has been thoroughly studied varying the inclination and orientation with respect to the Earth's magnetic field, and with and without the magnetic shielding of a mu-metal wire cage.

The detection efficiency, gain, P/V ratio, charge resolution, Transit Time (TT), and Transit Time Spread (TTS) were measured simultaneously with the aim of evaluating variations of the PMT characteristics changing the PMT relative orientations with respect to the Earth's magnetic field [13]. The PMT Z-axis was defined directed through the centre of the neck towards the photocathode, and the V-axis vertical downwards (see figure 4). The different angle of inclination (Φ in figure 4) was defined in terms of the angles between the Z-axis with respect to the fixed V-axis. The rotation was defined as the horizontally moving of the PMT Z-axis. The rotation angle (θ in figure 4) defined the Z position with respect to the North direction. The PMT under test was measured in three inclinations: vertically downwards ($\Phi = 0^\circ$), horizontal position ($\Phi = 90^\circ$) and 50° downwards ($\Phi = 50^\circ$). For all sets of measured parameters the minimum, maximum and average

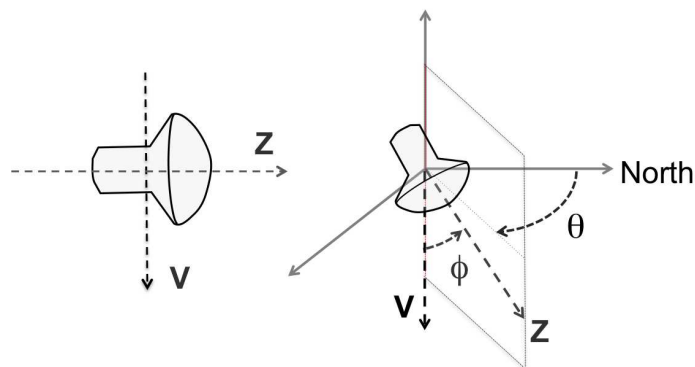


Figure 4. On the Left: PMT axis (Z) and the vertical axis (V). On the right: angle of inclination (Φ) and angle of rotation (θ).

values were measured, together with the variation, calculated as the percentage of the difference between maximum and minimum value, divided by the maximum [13].

Figures 5 to 9 show the measurements that exhibit the maximum variations for the measured parameter rotating the PMT. The discrepancy between the values measured in the position corresponding to 0° and 360° of the rotation angle are within the resolution of each different measurement which value is smaller than the symbol size.

As already reported in other studies [12, 14] the detection efficiency in unshielded (naked) large area PMTs is strongly degraded by the Earth's magnetic field, which influences the trajectory of photoelectrons especially between the photocathode and the first dynode. NEMO measurement results for the naked and shielded PMT are shown in figure 5, where all values are normalized to the maximum one. These results indicate that while varying the PMT orientation, the maximal detection efficiency variation, the percentage of the difference between the maximum and minimum value divided by the maximum, is about 40% for a naked PMT. The use of the magnetic shielding considerably reduces the variations that become smaller than 6%. Considering all the measurements in the three inclinations, the average variation of the detection efficiency was about 25% on a naked PMT, which decreases up to 4% using the mu-metal cage.

Large variations, up to the maximum value of 29%, were also measured in the gain of the unshielded PMT, as shown in figure 6. In this case, the magnetic shielding reduces these variations to less than 7%.

The average gain variation measured in different inclinations was about 24% for a naked PMT, reduced by the mu-metal cage up to 6%. Large variations (up to 41%) in the P/V ratio were measured for the unshielded PMT (figure 7). The magnetic shielding reduces the variations, down to 14% and increases the P/V average value, a ratio. Considering all the different inclinations, the mean P/V variation measured for an unshielded PMT was about 30%, which decreases to 13% with the mu-metal cage.

As far as charge resolution measurements are concerned, large effects induced by the magnetic field were measured for the unshielded PMT, with variations up to 50%. The mu-metal cage reduced the variations to less than 20%. As shown in figures 6 and 8, the measurements of the gain and of the charge resolution for the same angle of inclination are fully coherent, considering as at

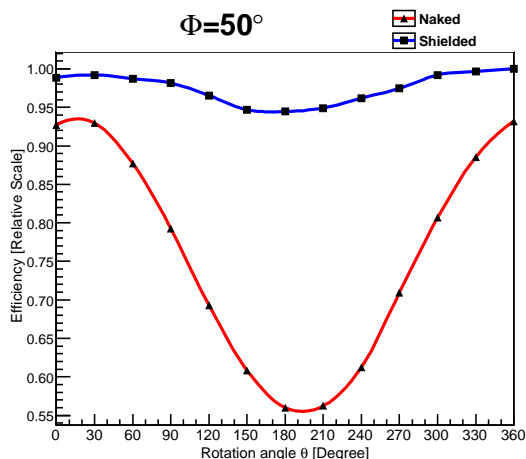


Figure 5. Variation of detection efficiency (normalized to the maximum measured value) for a PMT oriented downwards at the inclination of $\Phi = 50^\circ$ from the vertical. Triangles: naked PMT; squares PMT with the shielding of a mu-metal cage. The lines only guide the eye.

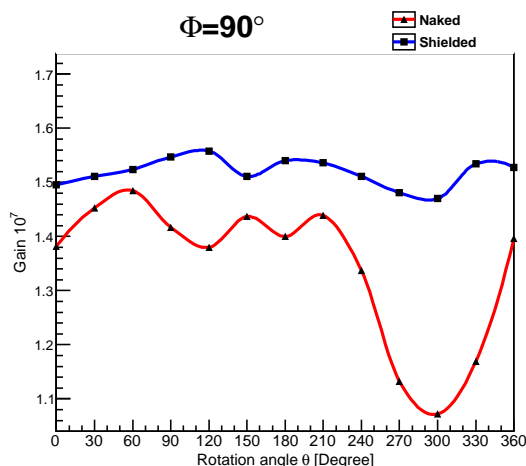


Figure 6. Variation of the gain for a PMT horizontally oriented ($\Phi = 90^\circ$). The symbols are the same as in figure 5.

the same rotation angle (300°) these parameters had the worst values.

As regards the mean variation of the charge resolution for the various inclinations, a value of about 44% was measured on a naked PMT, reduced by the magnetic shield to 18%.

Transit Time measurements did not show a significant dependence on the relative PMT orientation to respect the Earth's magnetic field: the maximum variation was less than 500 ps for the unshielded PMT, and got even smaller when using the mu-metal cage. Variations up to 20% in TTS were measured for the unshielded PMT (see figure 9), while the mu-metal cage strongly reduced this effect, up to 2%. The mean variation of the TTS for the different inclinations measured in a naked PMT was about 11%, reduced to 4% by using the magnetic shielding. Nevertheless, no significant improvements in the average TTS measurements were found.

The fraction of spurious pulses does not significantly depend on the Earth's magnetic field.

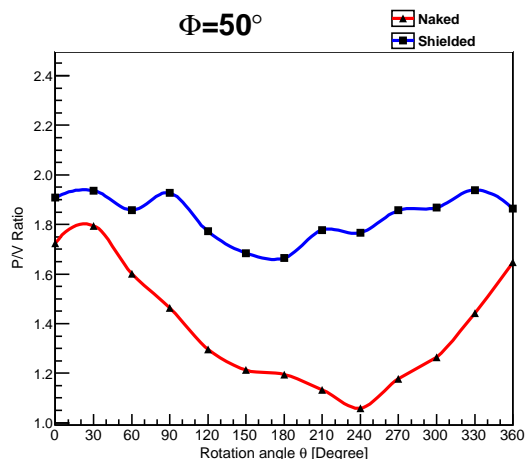


Figure 7. Variation of the Peak to Valley (P/V) ratio for a PMT oriented downwards at $\Phi = 50^\circ$ from the vertical. The symbols are the same as in figure 5.

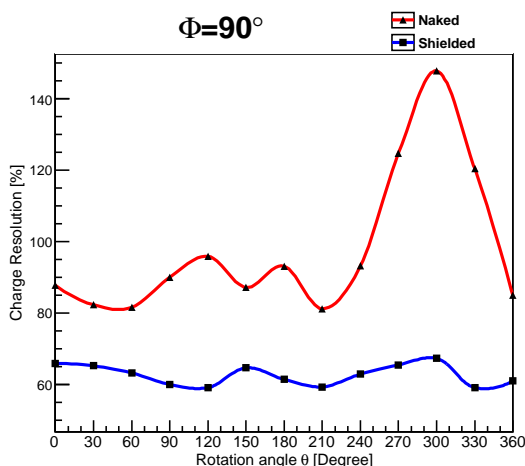


Figure 8. Variation of the charge resolution (σ) for a PMT horizontally oriented ($\Phi = 90^\circ$). The symbols are the same as in figure 5.

Conversely, delayed-pulses do have a significant dependence on the magnetic field. Also in this case the mu-metal cage greatly improves the PMT performance. In conclusion, the results confirmed that the performance of large area PMTs is significantly affected by its orientation with respect to the Earth's magnetic field. Therefore, for the optical module described in this paper, the use of a mu-metal cage is mandatory. The passive magnetic shield adopted for the NEMO optical modules, as in other experiments [8], has the following characteristics: 1 mm-diameter mu-metal wire, a nickel-iron alloy with high magnetic permeability ($\approx 10^5$). The cage (produced by ITEP⁵) is composed of two parts. A hemispherical part (30 cm diameter, 14 cm height) surrounding the entire photocathode area, and a flat part, a 30 cm diameter disk with a hole in its centre through which the PMT neck could fit. The scale of the grid is $68 \cdot 68 \text{ mm}^2$, giving a shadow effect on the

⁵Institute for Theoretical and Experimental Physics, Moscow, <http://www.itep.ru>

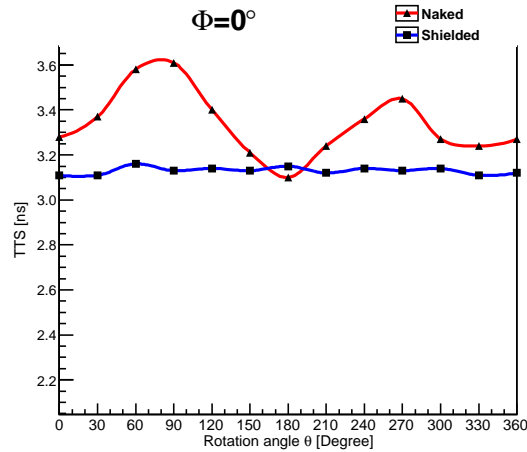


Figure 9. Variation of the Transit Time Spread (FWHM) for a vertically downwards-oriented PMT ($\Phi = 0^\circ$).

photocathode smaller than 4% and a reduction of the measured magnetic field of a factor about four inside the volume of the cage.

2.5 The optical coupling

The optical gel inside the OM has a twofold effect: it creates the optical coupling between the PMT photocathode and the glass sphere, and ensures the mechanical assembly of the PMT with the glass sphere and the mu-metal cage. The main requirements for the optical gel were:

- high transparency;
- a refractive index close to the ones of the glass sphere and sea water;
- a good rigidity to hold the OM components, with sufficiently elastic properties to absorb shocks and to accommodate for the deformation of the glass sphere under pressure;
- stability of the optical and mechanical characteristics over more than 10 years.

The selected material is a two-component (A and B) silicone gel, WACKER⁶SilGel 612. Following the same procedure described later in section 4, four mixtures with different combinations of the two components were produced varying the volumetric ratio (40B:100A, 50B:100A, 60B:100A, 70B:100A) and their optical and mechanical properties were measured. The optical measurements, concerned the transmittance and the refraction index as a function of the light wavelength, are shown in figure 10.

Table 3 summarizes the measured values at 400 nm wavelength. The refraction index of the borosilicate glass of the transparent vessel in the range 350 ÷ 600 nm wavelength range is 1.48, the gel mixtures 50B:100A and 60B:100A provide the best optical matching. The resistance to the elongation under a load for the different four gel mixtures were measured by using OM prototypes, made by a PMT glued with the gel to a glass hemisphere. To test each gel mixture three different prototypes have been built. Each one was tested by applying an external load to the PMT along its central axis, as shown in figure 11.

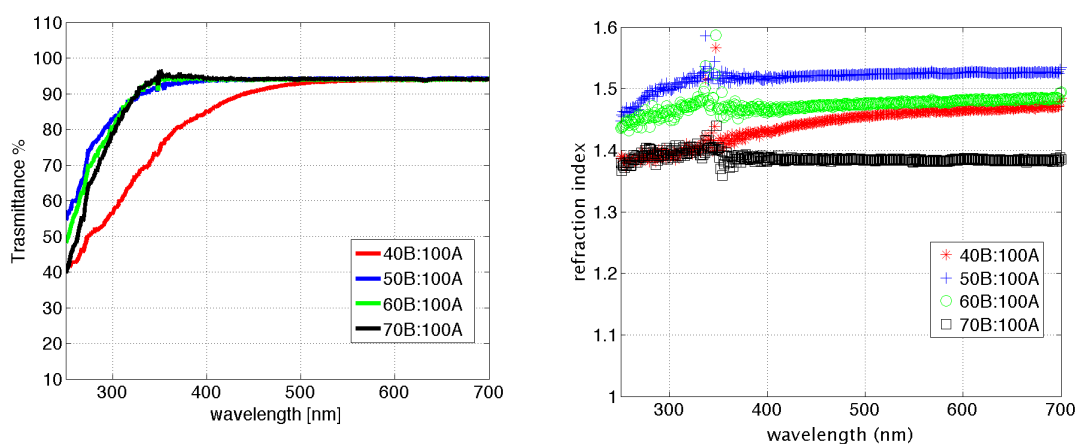


Figure 10. Transmittance (on the left) and the refractive index (on the right) for the different gel compositions.

Table 3. Optical properties measured for the 4 gel mixtures.

Gel Composition	40B:100A	50B:100A	60B:100A	70B:100A
Transmittance [%] (at 400 nm)	85	93.8	94.3	94.7
Absorption length [%] (at 400 nm)	12	30	33	35
Refraction index (at 400 nm)	1.43	1.50	1.47	1.38

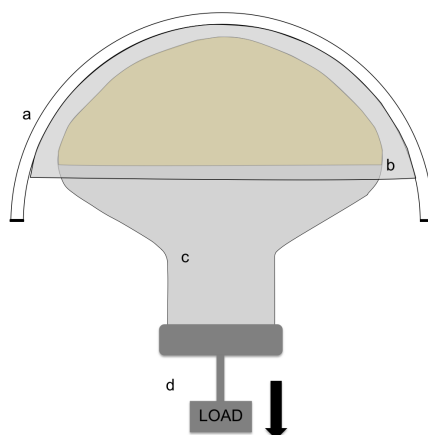


Figure 11. Sketch of the OM prototypes used for the load resistance tests for the different gel mixtures: (a) glass sphere, (b) gel, (c) PMT, (d) applied load.

In table 4 are given the mean value of the loads that caused detachments between the gel and the glass surface, degrading the optical coupling, normalized to the glued surface. For each value the error was about the 10%. The best result was obtained with the 50B:100A gel mixture.

⁶Wacker Chemie AG Hanns-Platz 4, 81737 München, Germany

Table 4. Mean value of the load normalized with the prototype glued surface that caused degrading in optical coupling for the different gel compositions.

Gel Mixture	40B:100A	50B:100A	60B:100A	70B:100A
Load / surface [kg/cm^2]	0.5	1.2	0.6	0.6

Taking into account both results obtained for the optical and the mechanical properties, the 50B:100A mixture was selected.

2.6 The front end module

The Front End Module board (FEM) is a $10 \cdot 10 cm^2$ square printed circuit board placed close to the PMT inside the glass sphere of the OM (see figure 1). The FEM digitizes the PMT analog signals, encodes and transmits the data to the Floor Control Module (FCM) that is located on each floor of the tower. Details may be found in [15]. This readout has to encode the information of the anode analog signal: the time when it was originated, the total charge and the pulse shape. The PMT signal is extracted from the ISEG board through a coaxial cable and conditioned by the analog front end. Then the signal is sampled, digitally converted and then stored by a FPGA. Almost all the slow control operations, such as parameter setting, sensor reading, PMT voltage power supply control, ISEG board voltage supply and FPGA programming, are accomplished by a Digital Signal Processor (DSP). An 8-bit resolution and a 200 MHz sampling frequency are sufficient for retaining all the needed information's, providing a good compromise between performance and power consumption. The signal is sampled using two 8-bit Fast Analog to Digital Converters running at 100 MHz staggered by 5 ns. This technique yields the desired sampling rate while at the same time allows a lower power dissipation than what required by a single 200 MHz ADC. The PMT signal is band-limited by an anti-aliasing filter that stretches the anode pulse width to 50 ns. To match the [0 - 5 V] input dynamic range to the 1.024 V input range of the ADCs, the signal level is shifted and compressed by a non-linear circuit, which applies a quasi-logarithmic law. The equivalent resolution obtained amounts to about 13 bits with a constant relative error.

2.7 The time calibration system

To reconstruct the muon track direction, a “time stamp” must be associated to each anode pulse (hit), i.e. the arrival time of the signal generated by the photons hitting the PMT. Consequently, a common timing is needed for the full apparatus and the delay of the individual OMs with respect to a fixed reference has to be accurately known. In order to determine such time offsets, a timing calibration system has been designed which is based on the delivery of optical signals at known times to each OM [16]. Such signals are generated by a fast optical pulser, called Tim-Cal, which is installed inside each OM (see figure 1). The short duration light pulses emitted by a commercial blue wavelength LED on board the Tim-Cal are injected into the PMT by means of an optical fibre mounted on the neck of the PMT, and directed towards the centre of the photocathode passing through the back of the PMT. Each Tim-Cal is connected and driven by a control module, the Tim-Control, hosted on each floor of the tower, which can drive the Tim-Cal pulsers inside the

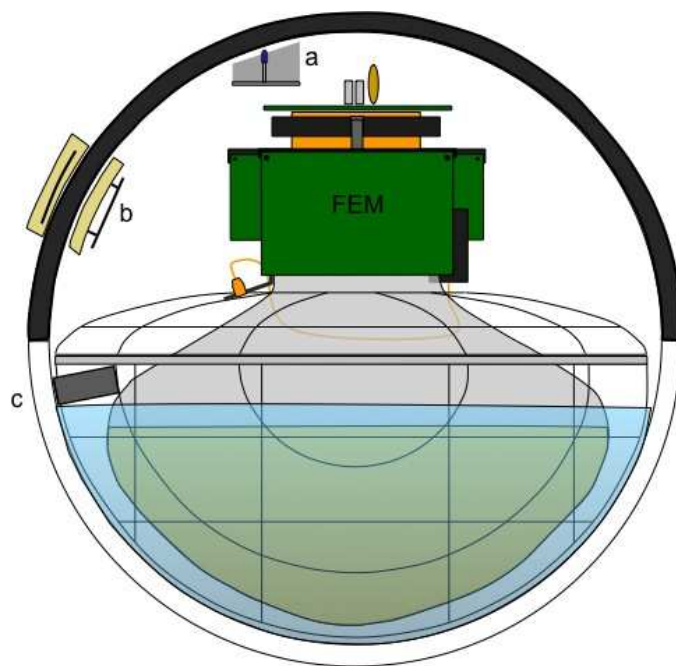


Figure 12. Schematic view of the ancillary new devices inside the experimental OMs (only one of them is mounted inside each OM). The view is turned of 90° with respect of figure 1: (a) LED beacon. (b) PORFIDO. (c) piezo-electric sensor.

optical modules of groups of adjacent floors. The time calibration system has been designed with a sub-nanosecond target accuracy in the determination of the OM time offsets.

3 Non-standard optical modules

14 OM of the 32 optical modules produced for the 8 storeys of the NEMO Phase-2 tower, host special devices to validate new technological solutions for future underwater neutrino detectors. Each of the two vertically downward-oriented OMs on the four lowest floors of the tower hosts a prototype LED beacon for time calibration purposes. The four horizontally oriented OMs on the top two storeys host an underwater oceanographic data measurement system, called PORFIDO. Finally, the two vertically downwards-oriented OMs on the topmost floor have two piezo-electric acoustic transducers to test a future acoustic positioning system. A schematic view of the position of these devices inside the optical modules is shown in figure 12. Only one of such devices could be mounted inside each experimental OM.

The two black half-spheres used for the two OMs with the piezo transducer device have two electrical connectors mounted. They were specially designed and equipped an additional connector. This allows to connect the piezo sensors to the electronics inside the FCM.

In the following sections a short description of each of these experimental devices is given.

3.1 PORFIDO

Gathering oceanographic data from a neutrino telescope installation can greatly benefit both oceanography and neutrino physics. A major request is that the installation of oceanographic probes should

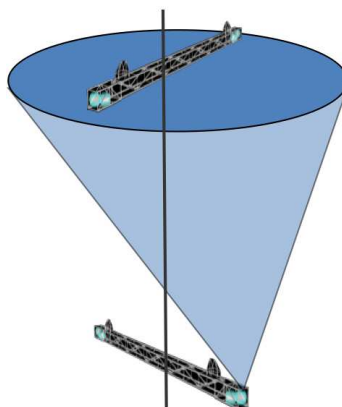


Figure 13. Scheme of light emission by a LED beacon.

not compromise the reliability of the neutrino telescope. In this aim the use of a limited number of external connectors is mandatory. Bearing this in mind, a novel underwater measurement system, called PORFIDO (Physical Oceanography by RFID Outreach) was designed and built. This device allows gathering oceanographic data (temperature, pressure, salinity, etc. . .) with a minimum of disturbance to the main neutrino detector installation [17]. Each PORFIDO device is composed of two elements: a sensor glued on the external surface of the OM, in contact with the seawater and a reader placed inside the sphere facing the sensor (see figure 12). Data are collected by the sensor and transmitted to the reader through the glass by means of RFID (Radio Frequency Identification). The sensor is built using a WISP⁷ (Wireless Internet Service Provider), an RFID tag developed at the Intel Research centre in Seattle that gathers power from the radio frequency, thus eliminating the need for batteries or connectors through the glass. The latest version of PORFIDO has a small size, $70 \cdot 40 \cdot 10 \text{mm}^3$ for the external sensor and about $70 \cdot 40 \cdot 10 \text{mm}^3$ for the reader inside the OM, easing its installation on the optical module.

3.2 LED beacon

The time calibration of a very large underwater detector, in addition to the standard time calibration system of NEMO (see section 2.7), can be performed by means of a system of optical beacons [18], i.e. a series of pulsed light sources distributed throughout the detector that illuminate large groups of optical modules (see figure 13). Their well-controlled light pulses can be used to closely monitor the time response of the optical modules as well as for studying the sea water properties.

The LED nano-beacons, mounted in the Phase-2 NEMO OMs, consist of two parts. A control board provides the required voltage to set the light intensity of the LED and the trigger signal, either from the outside (FEM board) or generated on the same board. The LED and the pulse generator circuit, which provides the electrical signal to enable the LED to flash, are mounted on a small PVC structure, which is glued near the centre of the upper hemisphere, directly on the internal surface of the optical module glass. The shape of the PVC structure takes into account the curvature of the glass sphere in order to allow the LED to be positioned vertically (see figure 12). The black paint was removed from the inner surface of the glass in front of the LED. Eight upwards-orientated LED

⁷<http://wisp.wikispaces.com>

nano-beacons, of different wavelengths, have been integrated in the two downwards-orientated OMs on the lower 4 floors. Four 470 nm LEDs were mounted on the first two floors from the bottom, two 440 nm LEDs on the third floor, and two 400 nm LEDs on the fourth floor.

3.3 Piezo-electric acoustic transducers

The aim of this system is to determine the optical module relative position to the acoustic beacon long baseline system during detector operation [19]. The piezo system is based on experience with the AMADEUS system [20] in the ANTARES neutrino telescope [21] and is made of two parts: a piezo sensor and a main amplifier board [22].

The sensor consists of a piezo-electric ceramic disc made of Pz27 (\varnothing 18 mm, height 12 mm) with pre-amplification stages inside an aluminum tube (\varnothing 20.5 mm, height 30 mm). The piezo-electric sensor is connected via a three-lead electrical cable to the main amplifier board for signal transfer and power supply. The main amplifier board houses an additional amplification stage, an analogue filter and a differential line driver.

The filter performs anti-aliasing and suppresses low frequency noise while the differential line driver provides an amplified differential signal according to LVDS specifications for routing to the ADC board. The piezo-electric sensor is directly glued to the lower hemisphere of the optical module to acoustically couple the glass and the ceramic. Due to its small dimensions it is possible to place the piezo sensor close to the PMT inside the module near the equator.

If the OM is stimulated externally via an acoustic signal (e.g. from the acoustic positioning system or a neutrino interaction) the piezo-electric ceramic is subject to a charge displacement on its surfaces proportional to the applied force via the piezoelectric effect. This charge displacement is converted to a voltage signal via a charge sensitive amplifier and sent to the main amplifier board. One advantage of this acoustic system as compared to other conventional ones is the use of the same housing as the main detector device (i.e. the PMT), and thus reducing the complexity and the number of underwater connectors.

4 The optical module production procedures

A well-established procedure was defined and followed to assemble the OM components described above and to produce and test the OMs to be mounted on the tower. The operations were carried out at the INFN integration workshop located at the Department of Physics in Catania. The time for producing a single OM was about 4 h even if future productions could be optimized performing some operations simultaneously. This time does not include the optical gel polymerization (8 h at least) and the photomultiplier dark conditioning before the tests (6 h at least).

4.1 The optical module assembly

Two $1 \cdot 1 \cdot 1m^3$ Plexiglas vacuum boxes, equipped with a pumping system capable to reduce the pressure to 300 mbar in less than 2 minutes, were built. These boxes were used both for an out-gassing procedure of the optical gel and to close the two glass hemispheres. The main phases of the OM assembly procedure were:

- soldering the high voltage board onto the PMT leads, followed by a functional check switching the PMT ON and recording the anode signal shape on a digital oscilloscope;

- cleaning of the PMT surface, the inner surface of the transparent half-sphere and the mu-metal cage using optical paper and methyl alcohol. Particular care was adopted in cleaning of each wire of the mu-metal cage;
- positioning of the mu-metal cage inside the transparent hemisphere already positioned inside the vacuum box;
- 1 cycle of out-gassing of the mu-metal cages. It consists of a phase under vacuum at a pressure of 250 mbar (3 min.), followed by air re-entry;
- preparation of the gel mixture: 1.5 litre per OM, with 1.0 litre of the A component and 0.5 litre of the B component, poured into a plastic beaker and mixed using a special mixing tool at 120 turns/min for 5 minutes;
- pouring of mixed gel into the glass hemisphere with the mu-metal cage already inside;
- 3 cycles of out-gassing (3 min./cycle) to remove residual air-bubbles inside the gel, each one followed by a phase of air re-entry;
- positioning of the PMT inside the hemisphere with a positioning tool. The minimum distance between the PMT surface and the sphere is set at 1 cm;
- 3 cycles of out-gassing (3 min./cycle) remove the residual air-bubbles inside the gel, each one followed by air re-entry;
- polymerization of the gel at atmospheric pressure and room temperature for 8 h at least;
- electrical cabling and connection of the FEM and Tim-Cal, already mounted on the neck of the PMT by using a plastic support (see figure 1), with the twisted pairs of the inner part of the connector mounted on the black hemisphere;
- gluing of the support of the time calibration system optical fibre on the neck of the PMT using a silicone glue. Finally, the fibre is connected to each extremity using a FC connector (see figure 1).

4.2 The optical module testing

Before closing and sealing the optical module, a systematic check was performed on all the assembled OMs to verify the procedure and to assess the functionality of each element. A test-bench was set up to reproduce the operative connections and data transmission between each OM and the electronics control modules. Each assembled OM was positioned inside a light-tight dark box and switched on using a specific software. The full functionality of the electrical connections and the absence of interference between the electronic devices inside the OM were checked. Each PMT was switched on at its own nominal voltage and the dark current signal digitized through the Front End Module. The shape and the dark count rate of the pulses were measured, and the consistency with measurements on the PMT before assembly was checked. The functionality of the time calibration system was verified by switching on the LED at the calibrated intensity value. A study of the shape and the rate of the digitized PMT output signals allowed verifying the accuracy of the

intensity setting. All ancillary devices mounted inside the 14 experimental optical modules were checked by means of the test-bench described above and of the dedicated software. As far as the PORFIDO system is concerned, tests were also carried out to check that the RF field generated by the reader system did not interfere with the PMT or the electronics inside the OM.

4.3 The optical module sealing

The following step was the closure and sealing of the two halves composing the OM. The two hemispheres were positioned inside the vacuum box, aligned using a special tool, and joined so as to close the OM at an internal pressure of 250 mbar. In order to definitely protect and seal the optical module, an external sealing tape (TEROSTAT-81[®].⁸) was attached into the bevel along the two hemispheres, entirely onto the glass sphere. Later a corrosion protection tape (Scotchrap[®] 3M⁹) was applied on top of the TEROSTAT-81, and attached three times all around the glass sphere. As a precaution against problems in the OM closure, the assembled OMs were classified ready to be deployed only after a check that the internal pressure, measured by the pressure gauge, remained stable for at least 24 hours after closing.

4.4 Test under pressure

As a final step, 50% of the assembled OMs, randomly chosen, were checked in a hyperbaric chamber to test the water tightness and the mechanical resistance. Tests were carried out at the INFN-LNS NEMO workshop in Catania harbour. A well-defined pressure cycle, lasting almost 8 hours, with a constant pressure at 350 atm for more than 1 hour, was adopted. In none of such tests was found evidence for a change of the internal pressure or for a water leak into the OMs. Furthermore, no detachment of the optical gel from the inner surface of the glass sphere was observed.

5 Conclusions

A 13-inch diameter optical module with a large 10-inch PMT was designed as part of Phase-2 of the NEMO project. Each single component was chosen after intense R&D work on photomultipliers, high voltage supply circuit, optical coupling and effects of the Earth's magnetic shielding. Following a well-established production procedure, 32 OMs were assembled and their functionality tested both from an electrical and mechanical point of view by using test-benches and a hyperbaric chamber. Amongst the 32 optical modules assembled, 14 of them host experimental devices to validate technical solutions proposed for future underwater neutrino detectors.

Acknowledgments

The authors acknowledge U. Emanuele, D. Real, J. de Dios Zornoza and J. Zuñiga of the Paterna Instituto de Fisica Corpuscular (IFIC), Spain, for the development and construction of the LED beams and the Acoustics Group of the Erlangen Centre for Astroparticle Physics (ECAP), Germany, in particular A. Enzenhöfer, for the development and construction of the piezo-electric systems.

⁸Henkel AG& CO KGaA Henkelstr. 67, 40191 Dusseldorf, Germany

⁹3M Corporate Headquarters St. Paul, MN 55144-100, USA

References

- [1] M.A Markov, *On high energy neutrino physics*, in proceedings of Annual International conference of high energy physics, Rochester (1960).
- [2] F.Halzen, *Neutrino astronomy: An update*, *Astrop. Phys.* (2013) in press.
- [3] T. Chiarusi and M. Spurio, *High-Energy Astrophysics with Neutrino Telescopes*, *Eur. Phys. J. C* **65** (2010) 649.
- [4] KM3NeT Technical Design Report, ISBN 978-90-6488-033-9, <http://km3net.org/KM3NeT-TDR.pdf>
- [5] E. Migneco et al., *Status of NEMO*, *Nucl. Instrum. Meth. A* **567** (2006) 444.
- [6] The NEMO collaboration, G. Riccobene et al., *Deep seawater inherent optical properties in the Southern Ionian Sea*, *Astropart. Phys.* **27** (2007) 1.
- [7] The NEMO collaboration, S. Aiello et al., *Measurement of the atmospheric muon flux with the NEMO Phase-1 detector*, *Astropart. Phys.* **33** (2010) 263.
- [8] ANTARES collaboration, P. Amram et al., *The ANTARES optical module*, *Nucl. Instrum. Meth. A* **484** (2002) 369.
- [9] S. Aiello et al., *Procedures and results of the measurements on large area photomultipliers for the NEMO project*, *Nucl. Instrum. Meth. A* **614** (2010) 206.
- [10] The NEMO collaboration, I. Amore et al., *NEMO: a project for a km³ underwater detector for astrophysical neutrinos in the Mediterranean sea*, *Int. J. Mod. Phys. A* **22** (2007) 3509.
- [11] S. Aiello et al., *Aging characterization on large area photo-multipliers*, *Nucl. Instrum. Meth. A* (2012) in press.
- [12] E. Calvo et al., *Characterization of large area photomultipliers under low magnetic fields: Design and performances of the magnetic shielding for the Double CHOOZ neutrino experiment*, *Nucl. Instrum. Meth. A* **621** (2010) 222.
- [13] S. Aiello et al., *Influence of the Earth's Magnetic Field on large area photomultipliers*, *IEEE Trans. Nucl. Sci.* **59** (2012) 1259.
- [14] A. Tripathi, *A systematic study of large PMTs for Auger surface detectors*, 3rd Beane Conference, 17-21 June 2002, France.
- [15] The NEMO collaboration, F. Ameli et al., *The data acquisition and transport design for NEMO Phase-1*, *IEEE Trans. Nucl. Sci.* **55** (2008) 233.
- [16] The NEMO collaboration, M. Ruppi et al., *Timing calibration for the NEMO (NEutrino Mediterranean Observatory) prototype*, *IEEE Nucl. Sci. Symp. Conf. Rec.* **N15-293** (2007) 709.
- [17] M. Cordelli et al., *PORFIDO: Oceanographic data for neutrino telescopes*, *Nucl. Instrum. Meth. A* **626-627** (2011) 109.
- [18] The ANTARES collaboration, M. Ageron et al., *The ANTARES optical beacon system*, *Nucl. Instrum. Meth. A* **578** (2007) 498.
- [19] F. Simeone and S. Viola, *The SMO project: a submarine multidisciplinary observatory in deep-sea*, *IEEE 8th Int. Conf. Mobile Adhoc and Sensor Systems (MASS)*, (2011) pp. 898-903,
- [20] The ANTARES collaboration, J.A. Aguilar et al., *AMADEUS-The acoustic neutrino detection test system of the ANTARES deep-sea neutrino telescope*, *Nucl. Instrum. Meth. A* **626-627** (2011) 128.

- [21] ANTARES collaboration, M. Ageron et al., *ANTARES: the first undersea neutrino telescope*, *Nucl. Instrum. Meth. A* **656** (2011) 11 [[arXiv:1104.1607](#)] [[INSPIRE](#)].
- [22] A. Enzenhöfer, *Acoustic calibration for the KM3NeT pre-production module*, *Nucl. Instrum. Meth. A* (2012) in Press.